Cancer Research

AACR

Sodium Selenite Induces Superoxide-Mediated Mitochondrial Damage and Subsequent Autophagic Cell Death in Malignant Glioma Cells

Eun Hee Kim, Seonghyang Sohn, Hyuk Jae Kwon, et al.

Updated Version	Access the most recent version of this article at: doi:10.1158/0008-5472.CAN-06-4217
Supplementary Material	Access the most recent supplemental material at: http://cancerres.aacrjournals.org/content/suppl/2007/06/20/67.13.6314.DC1.html

Cited Articles	This article cites 49 articles, 18 of which you can access for free at: http://cancerres.aacrjournals.org/content/67/13/6314.full.html#ref-list-1
Citing Articles	This article has been cited by 8 HighWire-hosted articles. Access the articles at: http://cancerres.aacrjournals.org/content/67/13/6314.full.html#related-urls

E-mail alerts	Sign up to receive free email-alerts related to this article or journal.
Reprints and Subscriptions	To order reprints of this article or to subscribe to the journal, contact the AACR Publications Department at pubs@aacr.org.
Permissions	To request permission to re-use all or part of this article, contact the AACR Publications Department at permissions@aacr.org.

Research Article

Sodium Selenite Induces Superoxide-Mediated Mitochondrial Damage and Subsequent Autophagic Cell Death in Malignant Glioma Cells

Eun Hee Kim,[1] Seonghyang Sohn,[2] Hyuk Jae Kwon,[2] Seung U. Kim,[3,4] Min-Jung Kim,[5] Su-Jae Lee,[5] and Kyeong Sook Choi[1,3]

[1]Department of Molecular Science and Technology and [2]Lab of Cell Biology, Institute for Medical Sciences and [3]Brain Disease Research Center, Ajou University School of Medicine, Suwon, Korea; [4]Department of Neurology, University of British Columbia, Vancouver, British Columbia, Canada; and [5]Laboratory of Radiation Effect, Korea Institute of Radiological and Medical Sciences, Seoul, Korea

Abstract

Malignant gliomas are resistant to various proapoptotic therapies, such as radiotherapy and conventional chemotherapy. In this study, we show that selenite is preferentially cytotoxic to various human glioma cells over normal astrocytes via autophagic cell death. Overexpression of Akt, survivin, XIAP, Bcl-2, or Bcl-xL failed to block selenite-induced cell death, suggesting that selenite treatment may offer a potential therapeutic strategy against malignant gliomas with apoptotic defects. Before selenite-induced cell death in glioma cells, disruption of the mitochondrial cristae, loss of mitochondrial membrane potential, and subsequent entrapment of disorganized mitochondria within autophagosomes or autophagolysosomes along with degradation of mitochondrial proteins were noted, showing that selenite induces autophagy in which mitochondria serve as the main target. At the early phase of selenite treatment, high levels of superoxide anion were generated and overexpression of copper/zinc superoxide dismutase or manganese superoxide dismutase, but not catalase, significantly blocked selenite-induced mitochondrial damage and subsequent autophagic cell death. Furthermore, treatment with diquat, a superoxide generator, induced autophagic cell death in glioma cells. Taken together, our study clearly shows that superoxide anion generated by selenite triggers mitochondrial damage and subsequent mitophagy, leading to irreversible cell death in glioma cells. [Cancer Res 2007;67(13):6314–24]

Introduction

Gliomas account for >50% of all brain tumors and are by far the most common primary brain tumors in adults (1). Despite the use of conventional treatments, including surgery, γ-irradiation, and chemotherapy, the average life expectancy of glioma patients after the initial diagnosis is usually less than 1 year (2). Although caspase-mediated apoptosis is the best-defined cell death program counteracting tumor growth, glioma cells are resistant to the conventional proapoptotic cancer therapeutics (3). Therefore, effective treatment of malignant gliomas may rely on the development of novel strategies for inducing nonapoptotic cell death, such as autophagic cell death or cell death through mitotic catastrophe, which has been recently described as alternative death pathways (4).

Selenium, a metalloid element that occurs naturally in the earth's soil, is a key element for maintaining the activity of some antioxidant enzymes and redox-regulatory proteins (5). Several epidemiologic studies have shown an inverse association between selenium levels and cancer risks in humans (6–8), and selenium levels in the cerebrospinal fluid of patients with malignant brain tumors have been reported to be lower than those with benign tumors (9). Sodium selenite, a commonly used dietary form of selenium (10), was recently reported to confer anticancer effects through induction of apoptosis in several cancer cell types (11, 12). In this study, we show for the first time that selenite shows an anticancer effect via autophagic cell death in various glioma cells but not in astrocytes.

Autophagy, a regulated process of degradation and recycling of cellular constituents, also participates in organelle turnover and in the bioenergetic management of starvation (13, 14). During autophagy, parts of the cytoplasm or entire organelles are sequestered into double-membraned vesicles called autophagic vacuoles or autophagosomes. These autophagosomes ultimately fuse with lysosomes to generate single-membraned autophagolysosomes capable of degrading their contents. Although autophagy can serve as a protective mechanism against apoptosis and starvation by recycling macromolecules and removing damaged mitochondria and other organelles (15, 16), it can also lead to growth arrest, reduction in cell number, and a nonapoptotic cell death associated with appearance of excessive autophagic vesicles (17). Therefore, high levels of autophagy can function as a cell death effector mechanism. Recently, induction of autophagy or autophagic cell death has been reported in several types of cancer cells in response to radiation or chemotherapy (18, 19). The molecular mechanisms of autophagy remain largely unknown, including the initiating signal(s) of autophagy, the mechanism(s) by which the targeted organelle is recognized and/or selected by the autophagosome, the source(s) of the sequestering membrane, and the precise mechanism of vesicle formation.

In the present work, we present clear evidence that selenite-induced superoxide anion triggers functional and structural disruption in mitochondria, leading to mitochondria-selective autophagy (mitophagy) and subsequent nonapoptotic cell death. These findings provide novel insights into the underlying mechanisms of mitophagy, as well as offering a potential strategy for treatment of gliomas, which are resistant to proapoptotic therapeutics.

Materials and Methods

Cell culture. Human glioma cell lines U87MG, T98G, and A172 were purchased from Korean Cell Line Bank. Human glioma cell lines U343 and

U251 were purchased from the American Type Culture Collection. Various glioma cells were cultured in DMEM supplemented with 10% fetal bovine serum (FBS) and antibiotics (Life Technologies). The primary cultures of normal human astrocytes were prepared from 14-week-gestation fetal cerebrum tissues as described previously (20). Human astrocyte cultures were grown in DMEM with high glucose supplemented with 10% FBS and 20 μg/mL gentamicin (Life Technologies) and subcultured every 2 weeks, and cell culture passage number less than five was used in the present

study. Immunofluorescence study indicated that better than 99% of cells expressed glial fibrillary acidic protein, a cell type–specific marker for astrocytes. Permission to use human brain tissues for research was granted by the clinical screening committee involving human subjects of the University.

Chemicals. Sodium selenite, polyethylene glycol (PEG)-catalase, 3-methyladenine (3-MA), acridine orange, monodansylcadaverine (MDC), Cu (II)-(diisopropylsalicylate)₂ (CuDIPS), Mn (III) *meso*-tetrakis (4-benzoic
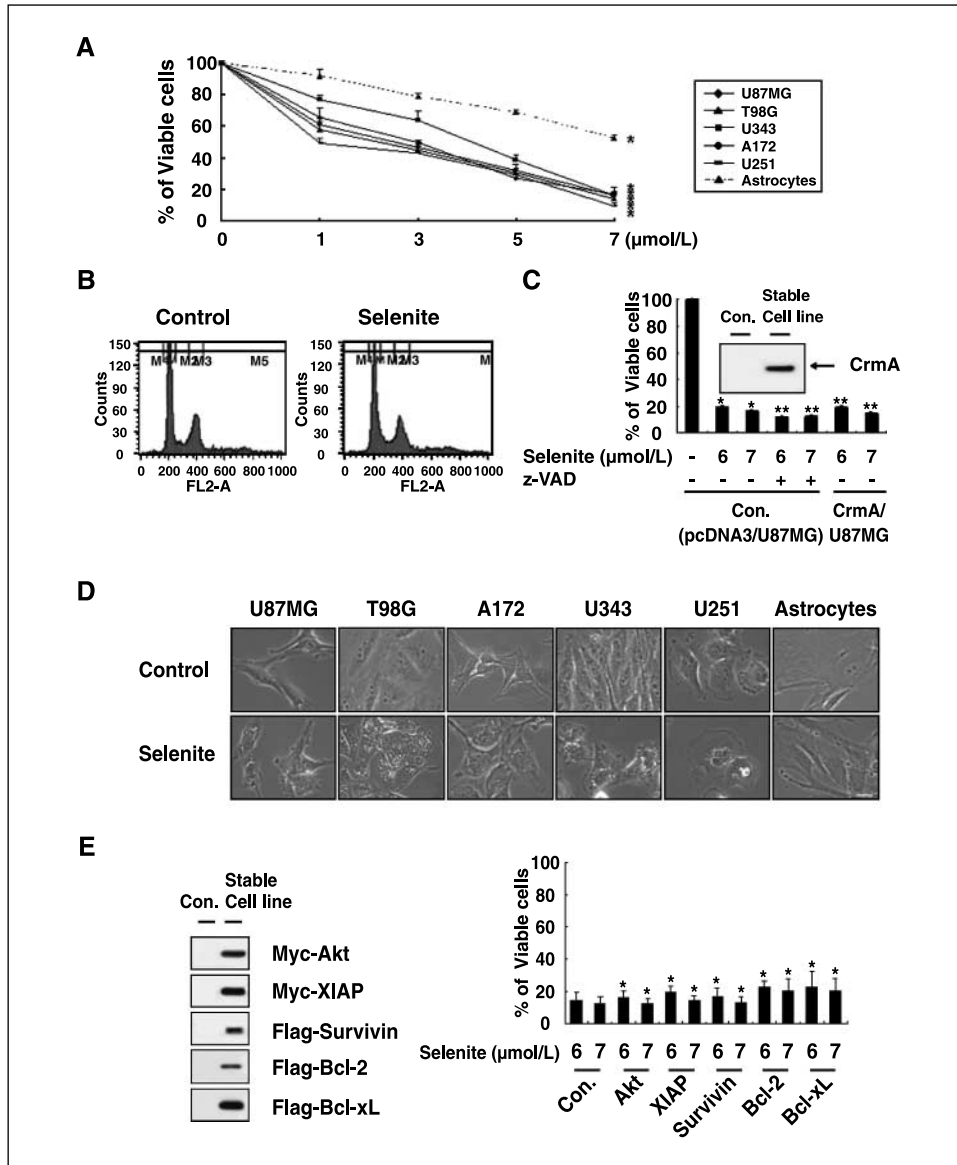

Figure 1. Sodium selenite induces caspase-independent nonapoptotic cell death in various malignant glioma cells but not in normal astrocytes. *A,* effect of selenite on the viability of human glioma cells and astrocytes. Human glioma cells and astrocytes were treated with the indicated concentrations of selenite for 24 h. Cellular viability was assessed using calcein-AM and EthD-1. *Points,* mean of three independent experiments; *bars,* SE. *, $P < 0.01$, compared with untreated cells. *B,* DNA content of glioma cells treated with selenite. U87MG cells were untreated or treated with 7 μmol/L selenite for 24 h, and DNA contents were measured by fluorescence-activated cell sorting analysis. *C,* inhibition of caspases by z-VAD pretreatment or CrmA overexpression does not block selenite-induced cell death. Con. cells (pcDNA3/U87MG; U87MG cells stably transfected with pcDNA3) were pretreated with 50 μmol/L z-VAD-fmk for 30 min and further treated with the indicated concentrations of selenite for 24 h. Cellular viability was assessed using calcein-AM and EthD-1. Stable U87MG cell lines overexpressing CrmA were established and CrmA expression was examined by Western blotting. Con. cells and CrmA-overexpressing U87MG cells were treated with selenite for 24 h, and cellular viabilities were compared using calcein-AM and EthD-1. *Columns,* average of three independent experiments; *bars,* SE. *, $P < 0.001$, compared with untreated cells; **, $P < 0.01$, compared with cells treated with selenite. *D,* morphologies of selenite-treated glioma cells and astrocytes. Various glioma cells and astrocytes were treated with 7 μmol/L selenite for 12 h and observed under a phase-contrast microscope. Bar, 2 μm. Representative pictures. *E,* effects of the overexpression of various antiapoptotic proteins on selenite-induced cell death. Stable cell lines overexpressing Myc-tagged Akt or XIAP, Flag-tagged survivin, Bcl-2, or Bcl-xL were established and their respective overexpressions were confirmed with Western blotting using anti-Myc or anti-Flag antibodies. Con. cells and the respective overexpressing cell lines were treated with 7 μmol/L selenite for 24 h and cellular viabilities were assessed using calcein-AM and EthD-1. *Columns,* average of three independent experiments; *bars,* SE. *, $P < 0.01$, compared with cells treated with selenite. To avoid problems of clonal variability, more than three different subclones of each overexpressing cell line were tested, and similar results were obtained in each case.
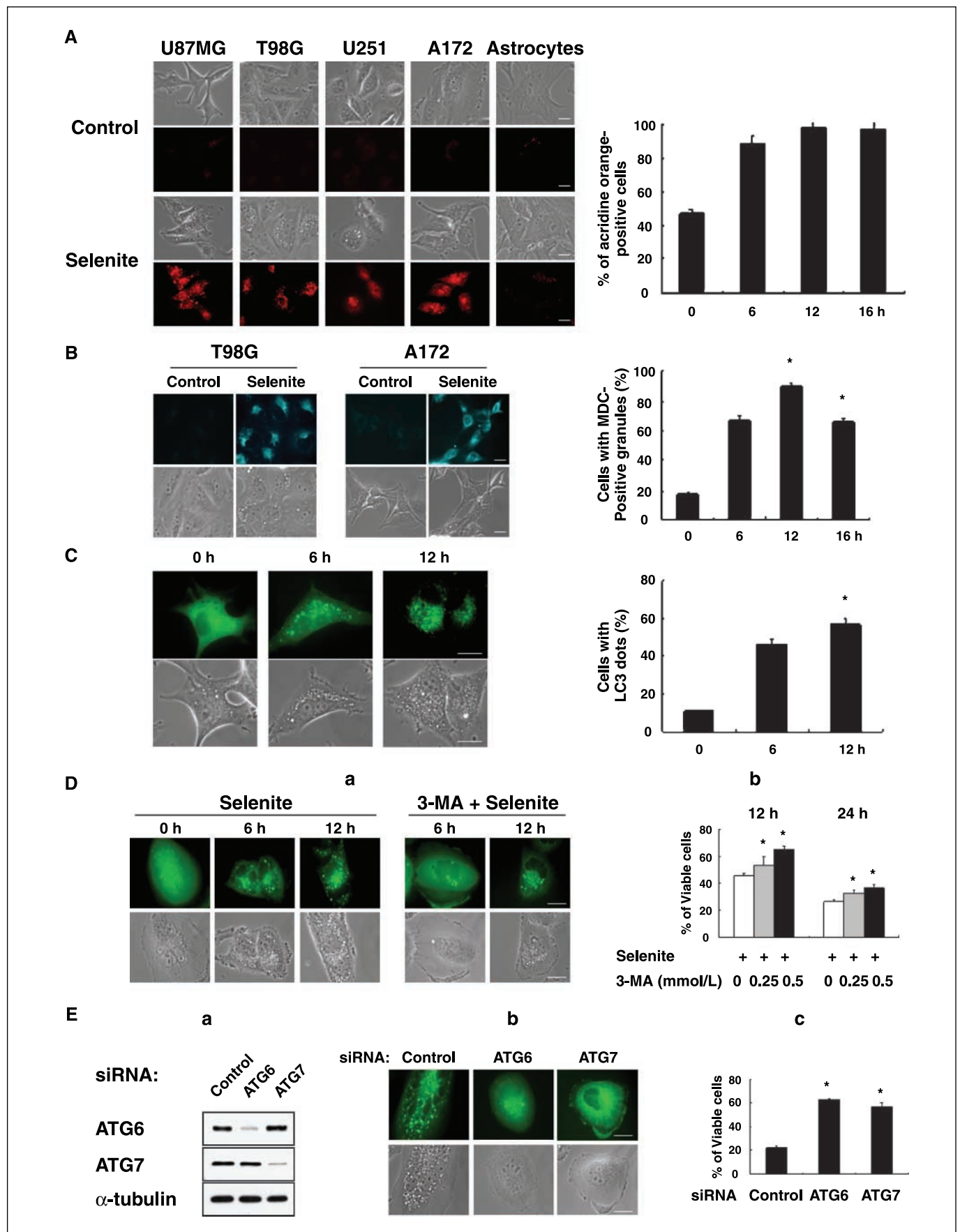
acid) porphyrin (MnTBAP), and *N*-acetylcysteine (NAC) were purchased from Sigma Chemical Corp. Hydroethidine, rhodamine 123 (Rh-123), calcein acetoxymethyl ester (calcein-AM), and ethidium homodimer (EthD-1) were purchased from Molecular Probes. Caspase inhibitor benzyloxy-carbonyl-Val-Ala-Asp-(OMe) fluoromethyl ketone (z-VAD-fmk) was from R&D Systems.

Measurement of cell viability. Cell viability was assessed by double labeling of cells with 2 μmol/L calcein-AM and 4 μmol/L EthD-1. The calcein-positive live cells and EthD-1–positive dead cells were visualized using a fluorescence microscope (Axiovert 200M using Axiovision Release 4.4 and Axiocam HRM digital camera, Zeiss).

Establishment of the stable cell lines overexpressing CrmA, Akt, Bcl-2, Bcl-xL, XIAP, survivin, copper/zinc superoxide dismutase, manganese superoxide dismutase, or catalase and the stable cell lines expressing the fluorescence specifically in mitochondria, endoplasmic reticulum, or peroxisomes. U87MG cells were transfected with the following: a mammalian expression vector containing CrmA cDNA, a vector containing Myc-tagged active Akt (Upstate Biotechnology), a vector encoding Flag-tagged Bcl-xL, a vector containing Flag-tagged Bcl-2, a vector containing Myc-tagged XIAP, a vector containing Flag-tagged survivin, and pcDNA3 (Invitrogen). The cDNAs encoding human copper/zinc superoxide dismutase (Cu/ZnSOD), manganese superoxide dismutase (MnSOD), and catalase were PCR amplified from plasmids containing these sequences (kindly provided by Dr. M. Akashi, National Institute of Radiological Sciences, Chiba, Japan), with the MnSOD- or catalase-specific primers designed to incorporate a 5′-hemagglutinin (HA) epitope. The respective PCR products were subcloned into the pcDNA3.1(+) expression vector (Invitrogen), and the resulting constructs were confirmed by nucleotide sequencing. U87MG cells were separately transfected with these generated expression vectors. Stable cell lines overexpressing CrmA, active Akt, XIAP, survivin, Cu/ZnSOD, MnSOD, or catalase were selected with fresh medium containing 500 μg/mL G418 (Calbiochem). Overexpression of CrmA, survivin, or Cu/ZnSOD was analyzed by Western blotting using anti-CrmA (BD PharMingen), anti-Flag (Sigma Chemical), or anti-Cu/ZnSOD (Calbiochem) antibody, respectively. Overexpression of MnSOD or catalase was analyzed by Western blotting using anti-HA antibody (Covance Research Products). Overexpression of active Akt or XIAP was analyzed by Western blotting using anti-Myc (Santa Cruz Biotechnology) antibody. Stable cell lines overexpressing Bcl-2 or Bcl-xL were selected in fresh medium containing 4 μg/mL puromycin (Sigma Chemical). Overexpression of Bcl-2 or Bcl-xL in the stable cell lines was analyzed by Western blotting using anti-Flag antibody. To establish the stable cell lines expressing the fluorescence specifically in mitochondria, endoplasmic reticulum (ER), or peroxisomes, U87MG cells were transfected with pEYFP-Mito, pEYFP-ER, or pEGFP-Peroxi vector (Clontech Laboratories) and selected with the complete medium containing 500 μg/mL G418.

Detection and quantification of acidic vesicular organelles with acridine orange staining. To detect acidic vesicular organelles (AVO), selenite-treated cells were stained with 1 μg/mL acridine orange for 15 min and samples were observed under a fluorescence microscope using Zeiss filter set #20 (excitation band pass, 546 nm; emission band pass, 575–640 nm). To quantify the development of AVOs, selenite-treated cells were stained with acridine orange, detached by trypsinization, and processed for the FACScan using CellQuest software (Becton Dickinson).

Visualization of autophagic vacuoles. Following treatment with selenite, autophagic vacuoles were labeled with MDC by incubating cells grown on coverslips with 50 μmol/L MDC in PBS at 37°C for 15 min. After incubation, cells were washed thrice with PBS and immediately analyzed by fluorescence microscopy using an inverted microscope (Axiovert 200M) equipped with Zeiss filter set #34 (excitation band pass, 390 nm; emission band pass, 460 nm).

GFP-LC3 translocation. U87MG and T98G cells were respectively transfected with the plasmid encoding GFP-LC3 (21), and the stable cell lines were selected with changes of medium containing 500 μg/mL G418. The stable cell lines expressing GFP-LC3 were incubated in the live cell chamber Chamlide IC (Live Cell Instrument) and then treated with 7 μmol/L sodium selenite. Translocation of GFP-LC3 from cytosol to autophagic vacuoles was observed under a fluorescence microscope equipped with Zeiss filter set #10 (excitation band pass, 450–490 nm; emission band pass, 515–565 nm), and the percentage of cells with GFP-LC3 dots was assessed.

Small interfering RNAs. The 25-nucleotide small interfering RNA (siRNA) duplexes used in this study were purchased from Invitrogen and have the following sequences: ATG6, CAGUUUGGCACAAUCAAUAA-CUUCA; ATG7, CAGAAGGAGUCACAGCUCUUCCUUA. Cells were transfected with siRNA oligonucleotides using LipofectAMINE 2000 (Invitrogen) according to the manufacturer's recommendations.

Measurement of mitochondrial membrane potential. Selenite-treated cells were stained with 1 μg/mL Rh-123 for 15 min, and samples were observed under a fluorescence microscope equipped with Zeiss filter set #10 (excitation band pass, 450–490 nm; emission band pass, 515–565 nm).

Transmission electron microscopy. Cells were prefixed in Karnovsky's solution [1% paraformaldehyde, 2% glutaraldehyde, 2 mmol/L calcium chloride, 0.1 mol/L cacodylate buffer (pH 7.4)] for 2 h and washed with cacodylate buffer. Postfixing was carried out in 1% osmium tetroxide and 1.5% potassium ferrocyanide for 1 h. After dehydration with 50% to 100% alcohol, the cells were embedded in Poly/Bed 812 resin (Pelco) and polymerized and observed under electron microscope (EM 902A, Zeiss).

Measurement of superoxide anion. Generation of superoxide was determined using a previously established fluorescence microscopy or flow cytometry technique based on the superoxide-induced conversion of hydroethidine to ethidium (22).

Figure 2. Induction of autophagy in glioma cells treated with selenite. *A,* selenite induces formation of AVOs in various glioma cells but not in astrocytes. Cells treated with 7 μmol/L selenite for 16 h were incubated with acridine orange and examined with an inverted fluorescence microscope using identical settings and image modifications. Bar, 2 μm. Representative fluorescent and phase-contrast images of the treated cells. AVOs were quantified with a fluorescence-activated cell sorter in T98G treated with 7 μmol/L selenite for the indicated times. *B,* selenite treatment increases the uptake of MDC in glioma cells. T98G or A172 cells were left untreated or treated with 7 μmol/L sodium selenite for 12 h and then stained with MDC. Images of the cells were taken on a fluorescence microscope. Bar, 2 μm. The number of cells with a granular positive MDC staining was counted; a minimum of 100 cells was counted per sample. *Columns,* average of three independent experiments; *bars,* SE. *, *P* < 0.01, compared with untreated cells. *C,* selenite triggers translocation of LC3 into granular structures in glioma cells. U87MG cell lines stably transfected with GFP-LC3 were treated with 7 μmol/L sodium selenite for the indicated times. Representative images of cells after fluorescence and phase-contrast microscopy. Bar, 2 μm. The percentage of cells with GFP-LC3 localized to granular structures was estimated by counting a minimum of 100 cells per sample with the given values representing the means of five independent experiments. *Bars,* SE. *, *P* < 0.01, compared with untreated cells. *D,* effect of 3-MA on selenite-induced LC3 translocation and cell death. *a,* T98G cells stably transfected with GFP-LC3 were pretreated or not with 0.5 mmol/L 3-MA for 30 min and further treated with 7 μmol/L sodium selenite for the indicated times to observe the translocation of GFP-LC3. Representative images of the cells observed under fluorescence and phase-contrast microscopy. Bar, 2 μm. *b,* effect of 3-MA on selenite-induced cell death. GFP-LC3–transfected T98G cells were pretreated or not with 3-MA at the indicated concentrations for 30 min and further treated with 7 μmol/L sodium selenite for 12 or 24 h. Cellular viabilities were compared using calcein-AM and EthD-1. *Columns,* average of three independent experiments; *bars,* SE. *, *P* < 0.05, compared with cells treated with selenite for the indicated time points. *E,* ATG6 and ATG7 are involved in selenite-induced LC3 translocation and cell death. *a,* GFP-LC3–expressing T87G cells were transfected with 40 nmol/L scrambled negative control RNA, ATG6 siRNA, or ATG7 siRNA and incubated for 24 h and expressions of ATG6 and ATG7 were analyzed by Western blotting. As a loading control, protein levels of α-tubulin were examined by Western blotting. *b,* GFP-LC3–expressing T98G cells were transfected with 40 nmol/L scrambled negative control RNA, ATG6 siRNA, or ATG7 siRNA and further treated with 7 μmol/L selenite for 12 h. Expression of GFP-LC3 in the respective cells was observed under fluorescence and phase-contrast microscope. Representative images of cells. Bar, 2 μm. *c,* GFP-LC3–expressing T98G cells were transfected as described above and further treated with 7 μmol/L selenite for 24 h. Cellular viabilities were analyzed using calcein-AM and EthD-1. *Columns,* average of three independent experiments; *bars,* SE. *, *P* < 0.001, compared with cells treated with selenite.
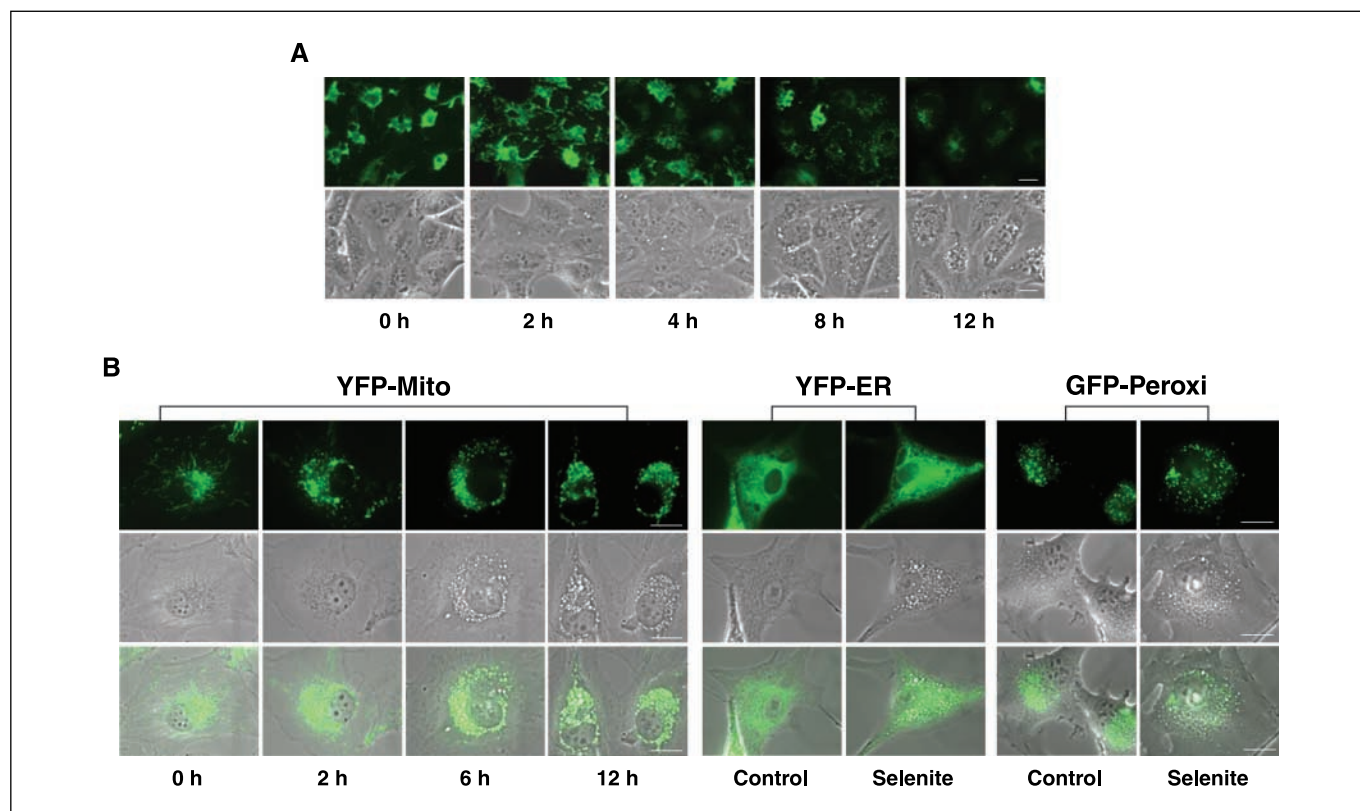
Figure 3. Selenite-induced autophagy is preceded by functional and structural disruption of mitochondria. *A*, reduction of MMP following selenite treatment. T98G glioma cells were treated with 7 μmol/L selenite for the indicated times and then incubated with Rh-123. Fluorescent and phase-contrast images of cells. Bar, 2 μm. *B*, mitochondria colocalize with vacuoles induced by selenite treatment, whereas the ER and peroxisomes do not. YFP-Mito cells were treated with 7 μmol/L selenite for the indicated times and observed under a fluorescence microscope. Bar, 2 μm. Fluorescent and phase-contrast images of cells are superimposed. To examine the effect of selenite on ER or peroxisomes, U87MG cell lines stably expressing the pEYFP-ER (YFP-ER cells) or pEGFP-Peroxi plasmid (GFP-Peroxi cells) were treated with 7 μmol/L selenite for 12 h and observed under a fluorescence microscope.

Measurement of SOD and catalase activity. Cells (2×10^6) plated in 100-mm culture dishes were collected, washed with PBS, and pelleted by centrifugation at $500 \times g$ for 10 min. The cell pellet was resuspended in ice-cold 50 mmol/L potassium phosphate (pH 7) containing 1 mmol/L EDTA, sonicated, and centrifuged at $10,000 \times g$ for 15 min at 4°C. The supernatant fraction was used for determination of SOD or catalase activity using kits from Cayman Chemical Co. according to the manufacturer's instructions.

Statistical analysis. All data are presented as mean ± SE of at least three independent experiments. The statistical significance of differences was assessed using ANOVA (GraphPad Software) followed by Student-Newman-Keuls' multiple comparison tests. $P < 0.05$ was considered significant.

Results

Sodium selenite induces nonapoptotic cell death in human glioma cells. We examined the effect of sodium selenite on viability in a variety of human glioma cells and normal astrocytes. Our results revealed that 1 to 7 μmol/L selenite decreased viability in the tested glioma cell lines, whereas the human astrocytes were relatively resistant to the same doses (Fig. 1*A*), suggesting that selenite is preferentially cytotoxic to malignant glioma cells over normal astrocytes. We next examined whether the cytotoxic effect of selenite on glioma cells is associated with induction of apoptosis. Flow cytometric analysis of the cellular DNA content showed that the sub-G_1 population was not increased in U87MG cells treated with 7 μmol/L selenite for 24 h (Fig. 1*B*), although cellular viability

decreased up to 20% at this time point (Fig. 1*A*). When we further assessed DNA fragmentation by terminal deoxynucleotidyl transferase–mediated dUTP nick end labeling (TUNEL) assay, TUNEL-positive cells were rarely found in T98G cells treated with 7 μmol/L selenite for 24 h (Supplementary Fig. S1). Selenite-induced cell death was not inhibited by pretreatment with the pan-caspase inhibitor z-VAD or by overexpression of the viral caspase-8 inhibitor CrmA (Fig. 1*C*; ref. 23). Selenite-treated glioma cells showed numerous small vesicles around their nuclei before selenite-induced cell death, whereas treated astrocytes did not (Fig. 1*D*). However, no apoptotic morphologies, such as cellular shrinkage, formation of apoptotic bodies, membrane blebbing, and nuclear fragmentation, were observed during selenite-induced cell death. Malignancy and resistance to various conventional anticancer therapies of gliomas have been associated with Akt activation due to mutations in the PTEN pathway and high expression of XIAP or survivin (24–26). In addition, Bcl-2 and Bcl-xL have been shown to protect various cancer cells from death stimuli (27). Accordingly, we investigated whether overexpression of these antiapoptotic proteins could attenuate selenite-induced cell death but found no evidence that selenite-induced cell death was affected by any of them (Fig. 1*E*). Taken together, selenite induces nonapoptotic cell death in human glioma cells but not in normal human astrocytes, suggesting that selenite treatment may provide an effective therapeutic strategy for malignant gliomas, many of which are resistant to conventional treatments due to inherent defects in apoptotic machineries.

Selenite induces autophagy in glioma cells. We investigated whether the vacuolation observed in selenite-treated glioma cells was associated with autophagy. To identify the development of AVOs, which are characteristic of autophagy (19), we used the lysomotropic agent acridine orange. Staining with acridine orange followed by fluorescence microscopy revealed significant development of AVOs beginning 6 h after treatment in U87MG, T98G, U251, and A172 glioma cells, but no AVO development was observed in astrocytes by 16 h after treatment (Fig. 2*A*). To further assess the possibility of autophagy, we stained sodium selenite–treated and untreated glioma cells with MDC, an autofluorescent base that has been reported to accumulate in autophagic vacuoles (28). Fluorescence microscopy revealed that the sodium selenite–treated T98G and A172 cells showed high-intensity accumulation of MDC into granular structures, whereas untreated glioma cells did

not (Fig. 2*B*). Vesicular accumulation of LC3 (microtubule-associated protein 1 light chain 3) is a marker of autophagy, as recruitment of modified LC3 to the nascent autophagic vesicle is a common event in autophagosome formation (21). To reliably detect the formation of autophagic vesicles, we expressed GFP-tagged LC3 (21) in U87MG cells and examined changes in the expression of GFP-LC3 following selenite treatment. In untreated cells, GFP-LC3 showed diffuse expression, whereas in selenite-treated cells it showed ring-shaped pattern around the vacuoles at 6 h and a high-intensity punctate expression at 12 h (Fig. 2*C*). Similar results were obtained in T98G cells stably transfected with GFP-LC3 (Fig. 2*D, a*). The functional role of autophagy in selenite-induced cell death was investigated using 3-MA, the specific inhibitor of early stages of the autophagic process (29). Pretreatment of GFP-LC3–transfected U87MG cells with 3-MA attenuated
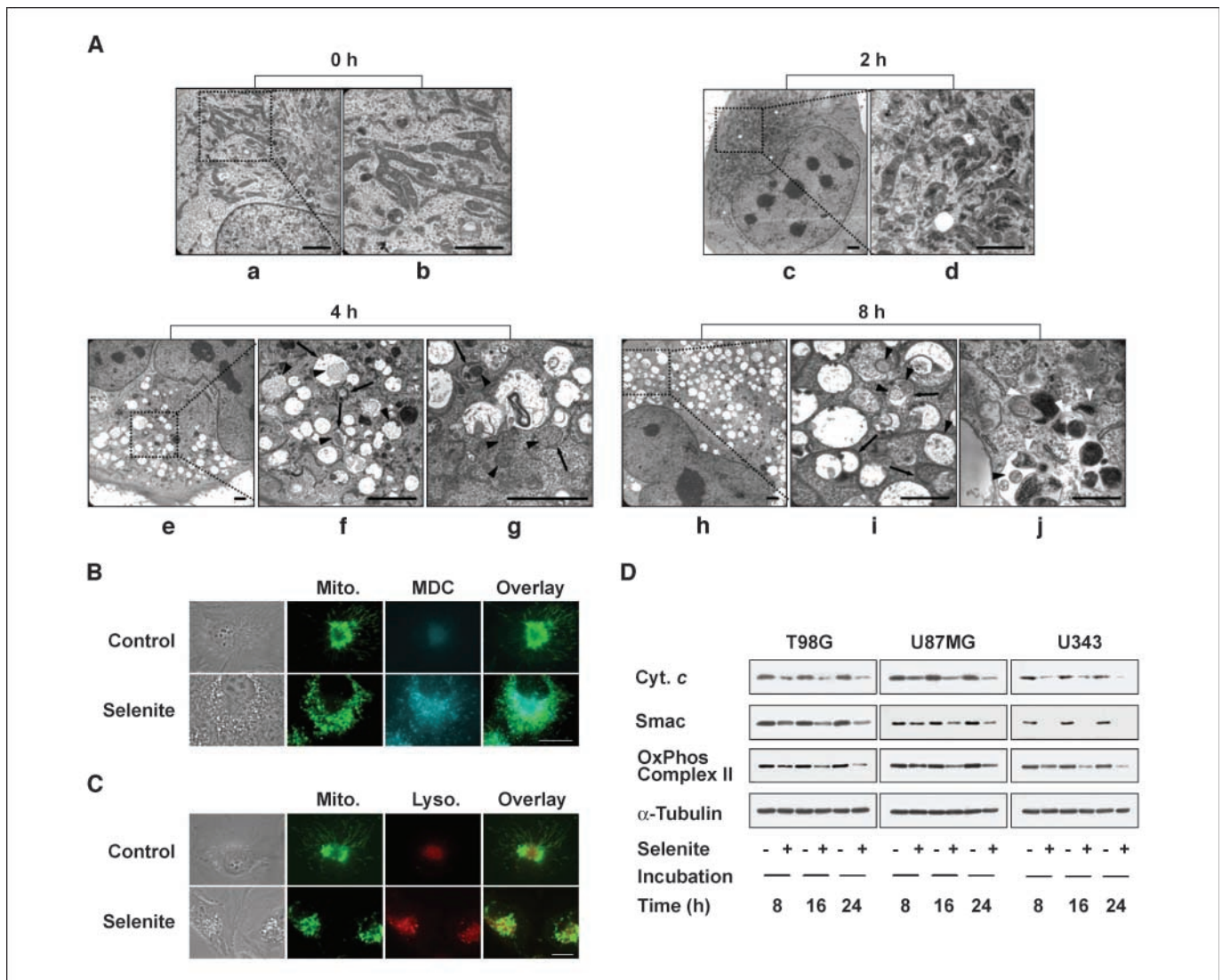

Figure 4. *A,* electron microscopic observation of glioma cells treated with selenite. T98G cells were untreated or treated with 7 μmol/L selenite for the indicated times and transmission electron microscopy was done. Bar, 2 μm. *B,* mitochondria (*Mito.*) and autophagic vacuoles may fuse after selenite treatment. YFP-Mito cells were untreated or treated with 7 μmol/L selenite for 12 h and then incubated with MDC. Changes in mitochondrial morphologies and cellular MDC uptake were observed under a fluorescence microscope. Bar, 2 μm. *C,* mitochondria and lysosomes (*Lyso.*) may fuse after selenite treatment. YFP-Mito cells were left untreated or treated with 7 μmol/L selenite for 12 h and then incubated with LysoTracker Red. Changes in mitochondrial morphologies and lysosomes were observed under a fluorescence microscope. Bar, 2 μm. *D,* reduction of mitochondrial protein levels during selenite-induced cell death. T98G, U87MG, or U343 cells were treated with 7 μmol/L selenite for the indicated time points, lysed, and subjected to Western blotting for the indicated mitochondrial proteins. Equal loading of protein samples was confirmed by Western blotting using α-tubulin antibody.
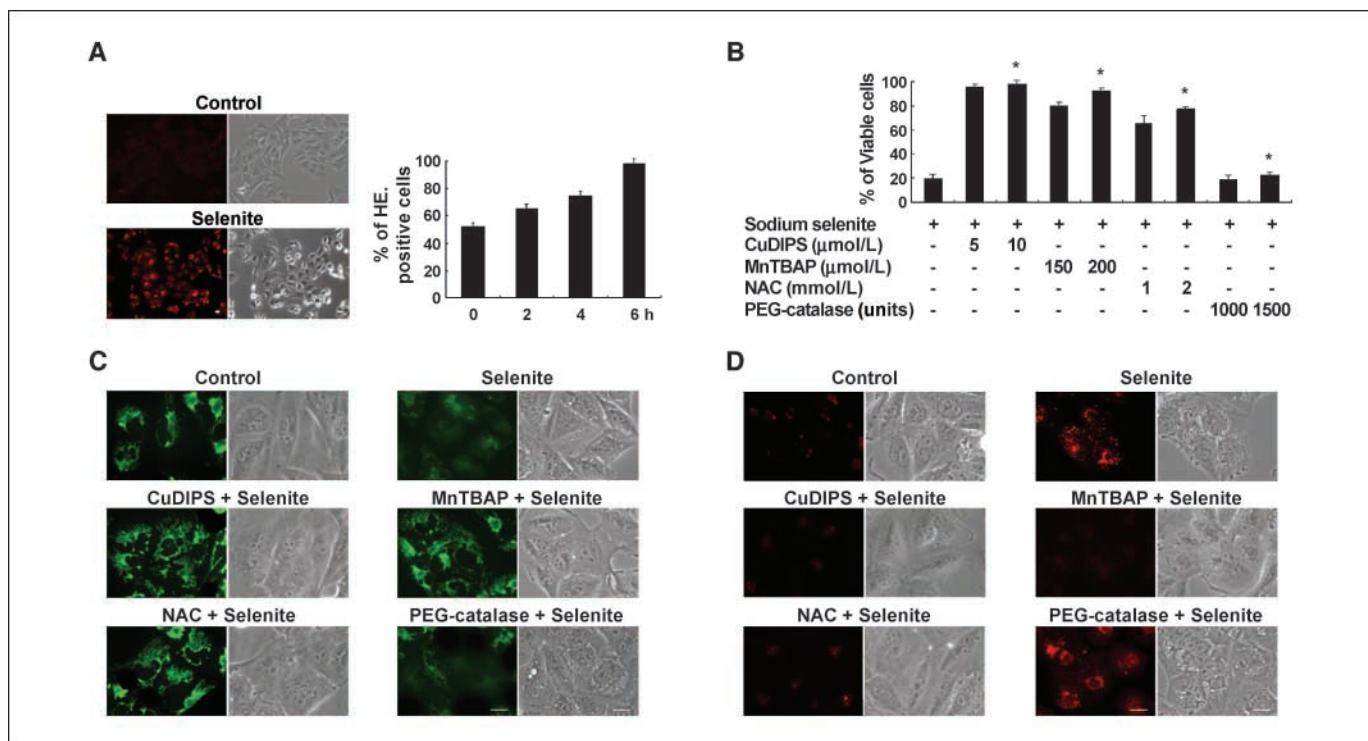
Figure 5. Pretreatment with CuDIPS, MnTBAP, or NAC blocks selenite-induced autophagic cell death. *A,* generation of superoxide by selenite. T98G cells were treated with 7 μmol/L selenite for 6 h, exposed to hydroethidine, and observed under a fluorescence microscope. Bar, 2 μm (*left*). The accumulation of intracellular superoxide levels was also measured in T98G cells following treatment with selenite for the indicated times and subsequent incubation with hydroethidine (*HE*) using a fluorescence-activated cell sorter (*right*). *B,* effect of various antioxidants on selenite-induced cell death. T98G cells were pretreated with the indicated concentrations of antioxidants for 24 h, and cellular viability was assessed using calcein-AM and EthD-1. *Columns,* average of three independent experiments; *bars,* SE. *, $P < 0.001$, compared with cells treated with selenite. *C,* pretreatment with CuDIPS, MnTBAP, or NAC blocks selenite-induced loss of MMP. T98G cells were treated with or without 10 μmol/L CuDIPS, 200 μmol/L MnTBAP, 2.5 mmol/L NAC, or 1,000 units PEG-catalase for 30 min, further treated with 7 μmol/L selenite for 8 h, and then incubated with Rh-123. Representative fluorescent and phase-contrast images of cells. Bar, 2 μm. *D,* pretreatment with CuDIPS, MnTBAP, or NAC blocks selenite-induced AVO formation. T98G cells were pretreated with or without 10 μmol/L CuDIPS, 200 μmol/L MnTBAP, 2.5 mmol/L NAC, or 1,000 units PEG-catalase for 30 min, further treated with 7 μmol/L selenite for 12 h, and then incubated with acridine orange. Representative fluorescent and phase-contrast images of cells. Bar, 2 μm.

selenite-induced translocation of GFP-LC3 and cell death (Fig. 2*D, a* and *b*). Furthermore, siRNA-mediated knockdown of either ATG6 or ATG7 expression also inhibited the translocation of GFP-LC3 and cell death induced by selenite (Fig. 2*E*), suggesting the involvement of ATG6 and ATG7 in selenite-induced autophagic cell death. Taken together, these results show that excessive autophagy induced by selenite contributes to nonapoptotic cell death.

Selenite-damaged mitochondria are targeted by autophagy. Because mitochondria play a crucial role in regulating cell death, we next examined whether selenite-induced autophagic cell death in glioma cells was associated with alterations in mitochondrial function and/or structure. Measurement of mitochondrial membrane potential (MMP) using Rh-123 showed that treatment of T98G cells with 7 μmol/L selenite induced a significant loss of MMP beginning 4 h after treatment (Fig. 3*A*). Interestingly, following exposure to selenite, decreased MMP was always detected in vacuolated cells. We then examined selenite-induced changes in mitochondrial morphology using an U87MG subline stably transfected with pEYFP-Mito plasmid for mitochondrial labeling (YFP-Mito cells). As shown in Fig. 3*B*, mitochondria in untreated YFP-Mito cells showed filamentous or elongated morphologies but became fragmented within 2 h after selenite treatment. Notably, all mitochondria exactly colocalized with the numerous small vacuoles 6 h after treatment. Beyond 6 h after treatment, the numbers and sizes of vacuoles expressing mitochondria-specific fluorescence

increased further. These results suggest the possibility that fragmented mitochondria by selenite treatment may be engulfed by autophagic vacuoles. To test whether the autophagic vacuoles also colocalized with the ER or peroxisomes during selenite-induced autophagy, we used a stable U87MG subline transfected with pEYFP-ER or pEGFP-Peroxi plasmid. In contrast with mitochondria, colocalization of the vacuoles with the ER or peroxisomes was minimal in selenite-treated cells, suggesting that mitochondria may be selectively targeted during selenite-induced autophagy. Transmission electron microscopy to observe ultra-structural changes showed that the mitochondria appeared as highly branched and interconnected tubular networks in untreated T98G cells (Fig. 4*A, a* and *b*). Two hours after treatment with selenite, however, the mitochondria appeared shorter and more rounded and the cristae were dramatically disrupted (Fig. 4*A, c* and *d*). From 4 h after treatment, swollen mitochondria filled with an electron-dense material, presumably mitochondrial remnants, were frequently observed (Fig. 4*A, e–j, black arrowheads*). Furthermore, these disorganized mitochondria were frequently surrounded by the double membrane associated with autophagosomes (Fig. 4*A, e–j* and *i, black arrows*). At 8 h after treatment, more advanced mitochondrial disruption was observed with frequent fusion between the vacuoles appearing to increase their sizes (Fig. 4*A, h* and *i*) and we observed ongoing fusion of autophagosomes with lysosomes (Fig. 4*A, j, white arrowheads*). Staining of selenite-treated
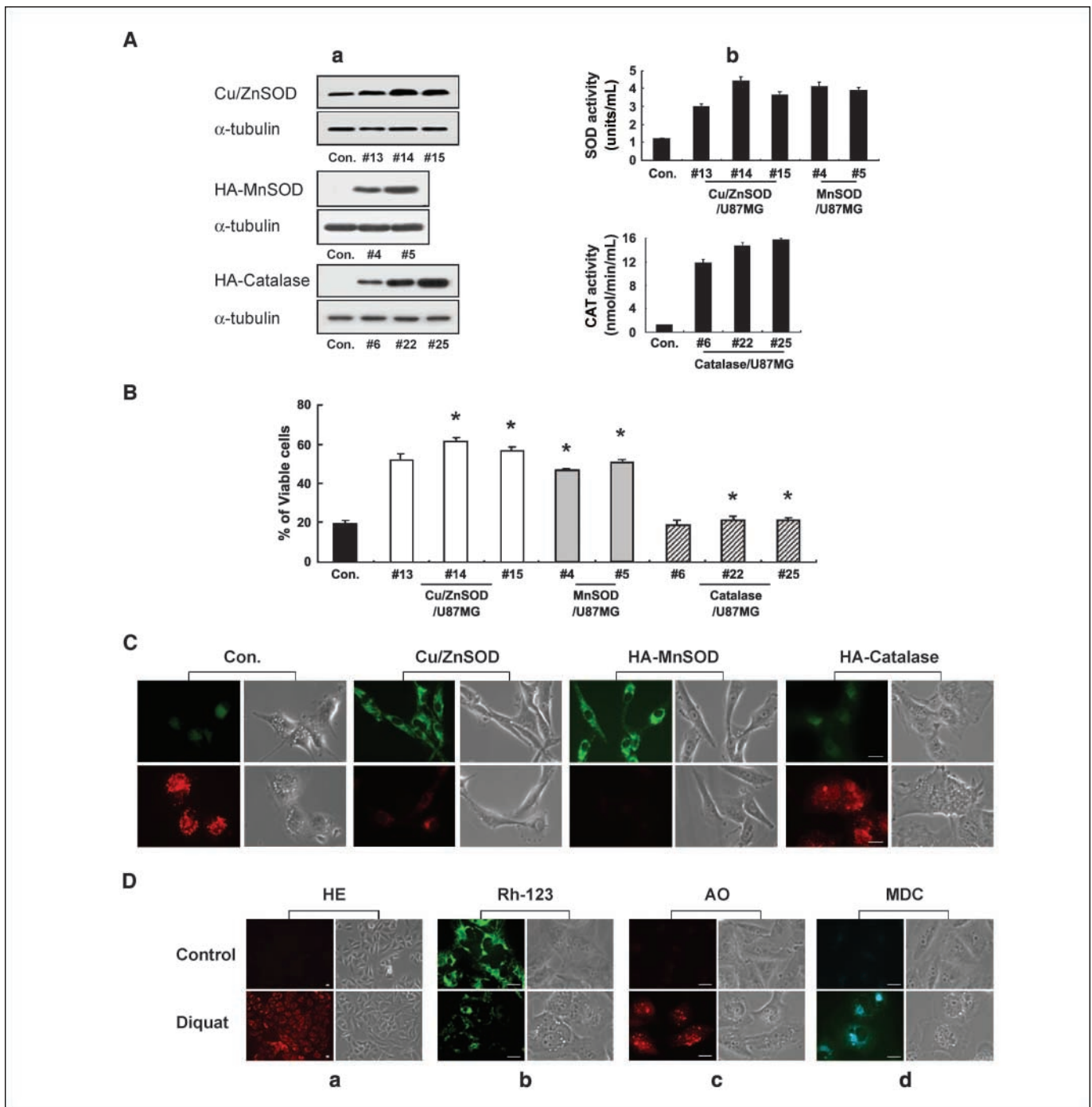
Figure 6. Selenite-induced autophagic cell death is blocked by overexpression of Cu/ZnSOD or MnSOD but not by catalase. *A, a,* establishment of the stable cell lines overexpressing antioxidant proteins. U87MG cells were stably transfected with expression vectors encoding Cu/ZnSOD, HA-MnSOD, or HA-catalase. As a control, Con. cells (U87MG cells transfected with pcDNA3) were used. Protein levels of the respective antioxidant proteins were analyzed by Western blotting using anti-Cu/ZnSOD or anti-HA antibodies, and equal loading of protein samples was confirmed by Western blotting of α-tubulin. *b,* Measurement of SOD and catalase (*CAT*) activity in the established stable cell lines. SOD activity in the lysates from the stable cell lines overexpressing Cu/ZnSOD or MnSOD was measured and compared with that of Con. cells using SOD assay kit (Cayman Chemical Co.). Representative results of three independent experiments. Catalase activity in the lysates from the stable cell lines overexpressing catalase was also compared with that of Con. cells using catalase assay kit (Cayman Chemical Co.). Similar results were obtained from three independent experiments. *B,* overexpression of SOD, but not catalase, blocks selenite-induced cell death. Con. cells and cells overexpressing Cu/ZnSOD, MnSOD, or catalase were treated with 7 μmol/L selenite for 24 h, and cellular viabilities were assessed using calcein-AM and EthD-1. *Columns,* average of three independent experiments; *bars,* SE. *, *P* < 0.001, compared with cells treated with selenite. *C,* overexpression of Cu/ZnSOD or MnSOD, but not catalase, blocks selenite-induced loss of MMP and autophagy. Con. cells and cells overexpressing Cu/ZnSOD (clone 15), MnSOD (clone 5), or catalase (clone 25) were treated with 7 μmol/L selenite for 8 h and then incubated with Rh-123. Representative fluorescent and phase-contrast images. Bar, 2 μm (*top*). The same cells were incubated with 7 μmol/L selenite for 12 h and then stained with acridine orange. Representative fluorescent and phase-contrast images. Bar, 2 μm (*bottom*). *D,* generation of superoxide by diquat induces autophagy. For detection of diquat-induced superoxide generation, T98G cells were treated with or without 10 μmol/L diquat for 12 h and then stained with hydroethidine. Representative fluorescent and phase-contrast images. Bar, 2 μm (*D, a*). For the detection of MMP loss or induction of autophagy, T98G cells were treated with or without 10 μmol/L diquat for 16 h and then stained with Rh-123, acridine orange (*AO*), or MDC. Representative fluorescent and phase-contrast images. Bar, 2 μm (*D, b–d*).

YFP-Mito cells with MDC or LysoTracker Red showed that the mitochondria significantly overlapped with the autophagic vacuoles and lysosomes, respectively (Fig. 4B and C). In addition, Western blot analysis revealed that the total amounts of mitochondrial proteins, such as cytochrome c, Smac, and OxPhos Complex II (succinate ubiquinol oxidoreductase) 70-kDa subunit, gradually decreased following selenite treatment (Fig. 4D). These results suggest that selenite-damaged mitochondria may ultimately be degraded via fusion with autophagosomes and lysosomes. Taken together, selenite may damage preferentially mitochondria in treated glioma cells, which then undergo autophagy to remove the disrupted mitochondria. However, excessive mitophagy may result in irreversible cell death.

Selenite-induced superoxide generation triggers mitochondrial damage and subsequent autophagic cell death. Next, we investigated the upstream regulatory mechanisms leading to selenite-induced mitochondrial damage and subsequent autophagic cell death. Selenite has been reported to increase the generation of superoxide anion during apoptosis (30, 31). Thus, we tested whether intracellular superoxide levels increase during selenite-induced autophagy in glioma cells. Hydroethidine-based measurements (22) revealed that intracellular superoxide levels were significantly increased in T98G cells from 2 h of selenite treatment compared with untreated cells (Fig. 5A). Similar trends were observed in luminometric analysis to detect superoxide levels using lucigenin (30) and H_2DCFDA-based detection of total reactive oxygen species (ROS) by fluorescence microscopy (data not shown). To examine whether superoxide plays a role in selenite-induced autophagic cell death, we pretreated T98G cells with various antioxidants and then exposed the cells to 7 μmol/L selenite for 24 h. Selenite-induced cytotoxicity was significantly blocked by pretreatment with a SOD mimetic CuDIPS or MnTBAP, whereas pretreatment with PEG-catalase could not block selenite-induced cell death (Fig. 5B). Pretreatment with NAC also showed a considerable blocking effect on selenite-induced cell death. Consistent with this finding, selenite-induced loss of MMP in T98G cells was significantly blocked by CuDIPS, MnTBAP, or NAC but not by PEG-catalase (Fig. 5C). Moreover, selenite-induced AVO formation was almost completely inhibited by CuDIPS, MnTBAP, or NAC but not by PEG-catalase (Fig. 5D). SOD is able to reduce the superoxide radical into hydrogen peroxide (H_2O_2). Catalase catalyzes decomposition of H_2O_2 to ground-state O_2. Because SOD mimetics and PEG-catalase showed different effects on selenite-induced autophagic cell death, we further examined the effect of SOD or catalase by establishment of U87MG sublines stably overexpressing Cu/ZnSOD, MnSOD, or catalase (Fig. 6A, a). Overexpression of Cu/ZnSOD or MnSOD in U87MG cells resulted in the enhancement of SOD activity. In U87MG cells stably overexpressing catalase, increased catalase activity was measured (Fig. 6A, b). Interestingly, selenite-induced cell death was significantly blocked by overexpression of Cu/ZnSOD or MnSOD but not by catalase (Fig. 6B). Very similar results were obtained using retroviral vector system overexpressing Cu/ZnSOD, MnSOD, or catalase (Supplementary Fig. S2), clearly showing that the regulatory roles of SOD and catalase in selenite-induced cell death are different. Selenite-induced dissipation of MMP and development of AVOs were also blocked by overexpression of Cu/ZnSOD or MnSOD but not by catalase (Fig. 6C). Moreover, treatment of T98G cells with diquat, a superoxide generator, induced autophagy in a manner similar to selenite (Figs. 2A and B, 3A, and 5A), including increased superoxide levels (Fig. 6D, a), MMP loss

(Fig. 6D, b), and the formation of autophagic vacuoles (Fig. 6D, c and d). In contrast, treatment of T98G cells with various doses of H_2O_2, nitric oxide donor SNAP, or peroxynitrite donor SIN-1 did not induce any evidences of autophagy (data not shown). Taken together, these results show that superoxide generation plays a major role in selenite-induced mitochondrial damage and subsequent autophagy leading to irreversible cell death.

Discussion

Selenium is an essential trace element with potent chemopreventive effects against various cancers (5). Sodium selenite is a common dietary form of selenium (10). To date, research into the cytotoxic effects of selenite in various cancer cells has predominantly focused on its apoptosis-inducing effects (12, 30, 32). Interestingly, we herein show that treatment with selenite can effectively induce autophagy and subsequent nonapoptotic cell death in malignant glioma cells. Autophagy was traditionally believed to be a random, nonselective process through which cytoplasm and organelles are sequestered into autophagosomes and delivered to lysosomes for degradation. However, a new concept of selective autophagy has emerged in recent years. The identification of the yeast mitochondrial protein Uth1P, which is required for mitochondrial autophagy (mitophagy) but not for macroautophagy, provided evidence that mitochondria can be specifically targeted for degradation by autophagy (33). However, few previous reports have described selective removal of an entire cohort of mitochondria via autophagy in mammals (34, 35). In the present study, high-power transmission electron microscopy images show that selenite treatment induced rapid disruption of cristae and mitochondrial swelling. Decreased cellular retention of Rh-123 indicated that a mitochondrial permeability transition (MPT) was induced by selenite treatment. Fluorescence microscopic analysis using YFP-Mito cells, YFP-ER, or GFP-Peroxi cells and transmission electron microscopy showed that autophagic vacuoles subsequently entrapped the disorganized mitochondria preferentially over other organelles, such as the ER or peroxisomes. Furthermore, various mitochondrial proteins were degraded in the progression of selenite-induced autophagy. Collectively, these results show that selenite induces excessive mitophagy. It is not yet known how the mitochondria are specifically selected for autophagy following exposure to selenite. MPT has been proposed to trigger the engulfment of depolarized mitochondria by autophagy (36). Alternatively, oxidatively damaged proteins or lipids on the surface of the mitochondria in selenite-treated cells may provide an "eat me" signal, mediating digestion by highly active autophagic vacuoles. It is interesting to speculate on whether autophagic depletion of mitochondria is the direct cause of selenite-induced cell death. We presume that selenite-enhanced autophagic activity and subsequent removal of a cohort of mitochondria might contribute to irreversible cell death perhaps because a certain number of functional mitochondria are required for energy production and cell survival. Alternatively, selenite-induced autophagy of mitochondria may hasten the progression of nonapoptotic cell death by eliminating a major source of ATP production and decreasing the release of mitochondria-derived proapoptogenic factors, thus tipping the cellular balance away from apoptosis.

In terms of the mechanism by which selenite treatment affects the mitochondria, our results indicate that selenite-induced intracellular superoxide generation acts to trigger mitochondrial damage and subsequent autophagic cell death. Several lines of

evidence support this hypothesis. First, selenite-induced superoxide anion generation was accompanied by mitochondrial damage, including MMP dissipation, disruption of cristae, and fragmentation/swelling of mitochondria. Second, not only pretreatment with CuDIPS or MnTBAP but also overexpression of Cu/ZnSOD or MnSOD significantly blocked selenite-induced mitochondrial damage, formation of autophagic vacuoles, and ultimately cell death. Third, treatment with diquat, a superoxide generator, triggered mitochondrial damage and autophagic cell death in glioma cells. These findings indicate that superoxide plays a critical role in mitochondrial damage and subsequent autophagic cell death and may further suggest the existence of a positive amplification loop between superoxide generation and damaged mitochondria following selenite treatment. Recently, Yu et al. (37) showed that caspase inhibition induced autophagic cell death through ROS accumulation due to catalase degradation, suggesting that ROS damage can be a cause of autophagic cell death. Notably, however, PEG-catalase pretreatment and catalase overexpression did not block selenite-induced mitochondrial damage and autophagic cell death, suggesting that selenite-induced autophagic cell death is not associated with the regulation of catalase. Furthermore, H_2O_2, SIN-1, or SNAP treatment failed to induce autophagic cell death in glioma cells, whereas treatment with diquat induced autophagic cell death in these cells. These results suggest that superoxide, rather than other types of ROS, is responsible for selenite-induced mitochondrial damage and subsequent autophagy. A considerable protective effect of NAC on selenite-induced autophagic cell death might be due to its strong scavenger activity against ROS, including superoxide anion (38). Zhao et al. (32) recently showed that generation of superoxide during selenite-induced apoptosis in prostate cancer cells is dependent on p53. However, we found that selenite-induced superoxide generation and autophagic cell death occurred in glioma cells with both wild-type p53 (U87MG, A172, and U343; refs. 39, 40) and mutant p53 (T98G and U251; refs. 40, 41), indicating that generation of superoxide during selenite-induced autophagic cell death is not dependent on p53.

Our study revealed that 1 to 10 μmol/L selenite was preferentially toxic to various glioma cells over human normal astrocytes. Zhang et al. (42) previously reported that Wistar rats with brain gliomas given selenite-containing drinking water showed preferential selenite accumulation in tumor tissue versus normal brain. They also showed that dietary selenium decreased tumor development in rat transplanted with glioma (43). These results collectively suggest that intake of sodium selenite in human glioma patients may have a potential therapeutic effect for targeting malignant gliomas over normal brain cells. Although malignant gliomas are resistant to apoptosis (type I programmed cell death), they seem to be less able to resist autophagic cell death (type II programmed cell death; ref. 44). Notably, radiation, arsenic trioxide, and ceramide were shown to induce autophagy or autophagic cell death in various glioma cells (19, 45, 46), whereas these stimuli induced apoptosis in other types of cancer cells (47–49). We found that selenite-induced cell death in glioma cells was not blocked by overexpression of various antiapoptotic proteins, suggesting that sodium selenite–induced autophagic cell death pathway may be safely used in the treatment of malignant glioma cells, at least partially bypassing their dramatic resistance to various proapoptotic therapies. However, extensive animal studies and preclinical trials are required to warrant the potential applicability of selenite for treating resistant gliomas.

In summary, the present results show that the elevated levels of intracellular superoxide generated by selenite treatment of glioma cells initiated an autophagic cell death in which mitochondria served as the main target. These novel findings not only improve our understanding of the autophagic effect of selenite and the role of superoxide in this process but also offer a potential therapeutic strategy for malignant gliomas, which are resistant to various proapoptotic therapeutics.

Acknowledgments

References

1. Weller RO. Brain tumours in man. Food Chem Toxicol 1986;24:91–8.
2. Stewart LA. Chemotherapy in adult high-grade glioma: a systematic review and meta-analysis of individual patient data from 12 randomised trials. Lancet 2002;359:1011–8.
3. Lefranc F, Brotchi J, Kiss R. Possible future issues in the treatment of glioblastomas: special emphasis on cell migration and the resistance of migrating glioblastoma cells to apoptosis. J Clin Oncol 2005;23:2411–22.
4. Okada H, Mak TW. Pathways of apoptotic and non-apoptotic death in tumor cells. Nat Rev Cancer 2004;4:592–603.
5. McKenzie RC, Arthur JR, Beckett GJ. Selenium and the regulation of cell signaling, growth, and survival: molecular and mechanistic aspects. Antioxid Redox Signal 2002;4:339–51.
6. Cai L, You NC, Lu H, et al. Dietary selenium intake, aldehyde dehydrogenase-2 and X-ray repair cross-

complementing 1 genetic polymorphism, and the risk of esophageal squamous cell carcinoma. Cancer 2006;106:2345–54.
7. Li H, Stampfer MJ, Giovannucci EL, et al. A prospective study of plasma selenium levels and prostate cancer risk. J Natl Cancer Inst 2004;96:696–703.
8. Reid ME, Duffield-Lillico AJ, Sunga A, Fakih M, Alberts DS, Marshall JR. Selenium supplementation and colorectal adenomas: an analysis of the nutritional prevention of cancer trial. Int J Cancer 2006;118:1777–81.
9. El-Yazigi A, Al-Saleh I, Al-Mefty O. Concentrations of Ag, Al, Au, Bi, Cd, Cu, Pb, Sb, and Se in cerebrospinal fluid of patients with cerebral neoplasms. Clin Chem 1984;30:1358–60.
10. Schrauzer GN. Nutritional selenium supplements: product types, quality, and safety. J Am Coll Nutr 2001;20:1–4.
11. Sinha R, El-Bayoumy K. Apoptosis is a critical cellular event in cancer chemoprevention and chemotherapy by selenium compounds. Curr Cancer Drug Targets 2004;4:13–28.

12. Zhong W, Oberley TD. Redox-mediated effects of selenium on apoptosis and cell cycle in the LNCaP human prostate cancer cell line. Cancer Res 2001;61:7071–8.
13. Klionsky DJ, Emr SD. Autophagy as a regulated pathway of cellular degradation. Science 2000;290:1717–21.
14. Levine B, Klionsky DJ. Development by self-digestion: molecular mechanisms and biological functions of autophagy. Dev Cell 2004;6:463–77.
15. Bauvy C, Gane P, Arico S, Codogno P, Ogier-Denis E. Autophagy delays sulindac sulfide-induced apoptosis in the human intestinal colon cancer cell line HT-29. Exp Cell Res 2001;268:139–49.
16. Scott RC, Schuldiner O, Neufeld TP. Role and regulation of starvation-induced autophagy in the *Drosophila* fat body. Dev Cell 2004;7:167–78.
17. Tsujimoto Y, Shimizu S. Another way to die: autophagic programmed cell death. Cell Death Differ 2005;12:1528–34.
18. Kanazawa T, Germano IM, Komata T, Ito H, Kondo Y, Kondo S. Role of autophagy in temozolomide-induced

cytotoxicity for malignant glioma cells. Cell Death Differ 2004;11:448–57.

19. Paglin S, Hollister T, Delohery T, et al. A novel response of cancer cells to radiation involves autophagy and formation of acidic vesicles. Cancer Res 2001;61: 439–44.

20. Kim SU. Antigen expression by glial cells grown in culture. J Neuroimmunol 1985;8:255–82.

21. Kabeya Y, Mizushima N, Ueno T, et al. LC3, a mammalian homologue of yeast Apg8p, is localized in autophagosome membranes after processing. EMBO J 2000;19:5720–8.

22. Rothe G, Valet G. Flow cytometric analysis of respiratory burst activity in phagocytes with hydro-ethidine and 2′,7′-dichlorofluorescin. J Leukoc Biol 1990; 47:440–8.

23. Zhou Q, Snipas S, Orth K, Muzio M, Dixit VM, Salvesen GS. Target protease specificity of the viral serpin CrmA. Analysis of five caspases. J Biol Chem 1997; 272:7797–800.

24. Shingu T, Yamada K, Hara N, et al. Growth inhibition of human malignant glioma cells induced by the PI3-K-specific inhibitor. J Neurosurg 2003;98:154–61.

25. Wagenknecht B, Glaser T, Naumann U, et al. Expression and biological activity of X-linked inhibitor of apoptosis (XIAP) in human malignant glioma. Cell Death Differ 1999;6:370–6.

26. Chakravarti A, Noll E, Black PM, et al. Quantitatively determined survivin expression levels are prognostic value in human gliomas. J Clin Oncol 2002;20:1063–8.

27. El-Deiry WS. Role of oncogenes in resistance and killing by cancer therapeutic agents. Curr Opin Oncol 1997;9:79–87.

28. Biederbick A, Kern HF, Elsasser HP. Monodansylca-daverine (MDC) is a specific *in vivo* marker for autophagic vacuoles. Eur J Cell Biol 1995;66:3–14.

29. Seglen PO, Gordon PB. 3-Methyladenine: specific inhibitor of autophagic/lysosomal protein degradation in isolated rat hepatocytes. Proc Natl Acad Sci U S A 1982;79:1889–92.

30. Shen HM, Yang CF, Ong CN. Sodium selenite-induced oxidative stress and apoptosis in human hepatoma HepG2 cells. Int J Cancer 1999;81:820–8.

31. Shen HM, Yang CF, Ding WX, Liu J, Ong CN. Superoxide radical-initiated apoptotic signalling pathway in selenite-treated HepG(2) cells: mitochondria serve as the main target. Free Radic Biol Med 2001;30: 9–21.

32. Zhao R, Xiang N, Domann FE, Zhong W. Expression of p53 selenite-induced superoxide production and apoptosis in human prostate cancer cells. Cancer Res 2006;66:2296–304.

33. Kissova I, Deffieu M, Manon S, Camougrand N. Uth1p is involved in the autophagic degradation of mitochondria. J Biol Chem 2004;279:39068–74.

34. Lemasters JJ. Selective mitochondrial autophagy, or mitophagy, as a targeted defense against oxidative stress, mitochondrial dysfunction, and aging. Rejuvenation Res 2005;8:3–5.

35. Mijaljica D, Prescott M, Devenish RJ. Different fates of mitochondria: alternative ways for degradation? Autophagy 2007;3:4–9.

36. Elmore SP, Qian T, Grissom SF, Lemasters JJ. The mitochondrial permeability transition initiates autophagy in rat hepatocytes. FASEB J 2001;15:2286–7.

37. Yu L, Wan F, Dutta S, et al. Autophagic programmed cell death by selective catalase degradation. Proc Natl Acad Sci U S A 2006;103:4952–7.

38. Hussain S, Slikker W, Jr., Ali SF. Role of metal-lothionein and other antioxidants in scavenging super-oxide radicals and their possible role in neuroprotection. Neurochem Int 1996;29:145–52.

39. Li H, Lochmuller H, Yong VW, Karpati G, Nalbantoglu J. Adenovirus-mediated wild-type p53 gene transfer and overexpression induces apoptosis of human glioma cells independent of endogenous p53 status. J Neuropathol Exp Neurol 1997;56:872–8.

40. Asai A, Miyagi Y, Sugiyama A, et al. Negative effects of wild-type p53 and s-Myc on cellular growth and tumorigenicity of glioma cells. Implication of the tumor suppressor genes for gene therapy. J Neurooncol 1994;19: 259–68.

41. Zhao S, Tsuchiba T, Kawakami K, Shi C, Kawamoto K. Effect of As_2O_3 on cell cycle progression and cyclins D1 and B1 expression in two glioblastoma cell lines differing in p53 status. Int J Oncol 2002;21:49–55.

42. Zhang Z, Chinen Y, Zhu Z, Kimura M, Itokawa Y. Uptake and distribution of sodium selenite in rat brain tumor. Biol Trace Elem Res 1995;48:45–50.

43. Zhang Z, Kimura M, Itokawa Y. The decrement of carcinogenesis by dietary selenium and expression of placental from of glutathione-*S*-transferase in rat glioma. Biol Trac Elem Res 1997;57:147–55.

44. Lefranc F, Kiss R. Autophagy, the Trojan horse to combat glioblastomas. Neurosurg Focus 2006;20:E7.

45. Kanzawa T, Kondo Y, Ito H, Kondo S, Germano I. Induction of autophagic cell death in malignant glioma cells by arsenic trioxide. Cancer Res 2003;63:2103–8.

46. Daido S, Kanazawa T, Yamamoto A, Takeuchi H, Kondo Y, Kondo S. Pivotal role of the cell death factor BNIP3 in ceramide-induced autophagic cell death in malignant glioma cells. Cancer Res 2004;64: 4286–93.

47. Ross GM. Induction of cell death by radiotherapy. Endocr Relat Cancer 1999;6:41–4.

48. Gazitt Y, Akay C. Arsenic trioxide: an anti cancer missile with multiple warheads. Hematology 2005;10: 205–13.

49. Lin CF, Chen CL, Lin YS. Ceramide in apoptotic signaling and anticancer therapy. Curr Med Chem 2006; 13:1609–16.